Rock cliffs hazard analysis based on remote geostructural surveys: The Campione del Garda case study (Lake Garda, Northern Italy)

(Article begins on next page)

19 May 2024

UNIVERSITÀ DEGLI STUDI DI TORINO

1   Title

2   **Rock cliffs hazard analysis based on remote geostructural**

3   **surveys: the Campione del Garda case study (Lake Garda,**

4   **Northern Italy)**

5   Authors:

6   **Ferrero, A.M., Migliazza, M., Roncella, R., Segalini, A.**

7

8   Affiliation:

9   Department of Civil, Environmental and Territory Engineer and Architecture (DICATeA) –
10   University of Parma - V.le Usberti 181/a - 43124 Parma - Italy
11

12   Correspondance to:

13   Prof. Andrea Segalini
14   c/o Dept. Of Civil, Environmental and Territory Engineering and Architecture (DICATeA)
15   University of Parma
16   V.le Usberti 181/a
17   43124 Parma
18   Italy
19
20   Tel.   +39.0521.905952
21   Fax   +39.0521.905924
22   Email: andrea.segalini@unipr.it
23

24 **Abstract**

25 The town of Campione del Garda (located on the west coast of Lake Garda) and its access road

26 have been historically subject to rockfall phenomena with risk for public security in several areas of

27 the coast.. This paper presents a study devoted to the determination of risk for coastal cliffs and the

28 design of mitigation measures. Our study was based on statistical rockfall analysis performed with a

29 commercial code and on stability analysis of rock slopes based on the key block method. Hazard

30 from block kinematics and rock-slope failure are coupled by applying the Rockfall Hazard

31 Assessment Procedure (RHAP). Because of the huge dimensions of the slope, its morphology and

32 the geostructural survey were particularly complicated and demanding. For these reasons,

33 noncontact measurement methods, based on aerial photogrammetry by helicopter, were adopted. A

34 special software program, developed by the authors, was applied for discontinuity identification and

35 for their orientation measurements. The potentially of aerial photogrammetic survey in rock

36 mechanic application and its improvement in the rock mass knowledge is analysed in the article.

37

38 *Keywords*: rockfall hazard; remote geostructural survey; risk analysis; Campione del Garda;

39 Northern Italy.

40 **1   Introduction**

41 The rock fall phenomenon usually involves limited volumes of rock but it represents an element of

42 relevant hazard since it is a fast, sudden and, within the Italian territory is also a widespread

43 phenomenon. This problem assumes higher significance in the areas where urban settlements and

44 infrastructures have been developed in close proximity of rock cliffs.

45 Typical is the Lake Garda case, the widest Italian fresh water basin, located at the Alpine Arch base,

46 among the provinces of Brescia, Verona, Mantova and Trento.

47 The lake north-western shore is characterized by high and wide sub-vertical rock cliffs where an

48 important tourism activity is located giving to the lake shore an interesting economical importance.

49 The study regards the rock slope that overlooks the Campione del Garda inhabited shore, on the

50 west bank of the lake, frequently subjected to rock fall phenomena (Fig. 1).

51 The occurrence of several rock fall events drove the public administration to take steps in order to

52 improve the safety of this area characterized by an high risk increased by the presence of a well

53 developed tourist activity. Due to the morphological settings of the rock walls, the use of defence

54 systems to prevent block detachment, appeared not achievable so in order to choose and define the

55 most appropriate defence system an hazard assessment procedure was needed.

56

2 Geological setting

57

58 The surveyed area is, from the geological point of view, part of the Subalpine structural domain,
59 located in the central sector of the Southern Alps and constituted by folds and thrusts having a
60 primary direction E-W.

61 The main geological unit surfacing in the studied area is the Main dolomite constituted by a
62 succession of stratified dolomite limestones sometime marly limestone and thin marl and
63 bituminous layers followed by the proper dolomite unit in its grey, white and pink facies.

64 This Subalpine structural sector is formed by a single and relict palaeographic element: the
65 Lumbard Mesozoic basin which is characterized by homogeneous style of deformation, outcrop
66 shortening and wrinkling age. The studied area involves the eastern portion of such domain, where
67 the stratigraphic series are considerably thinner than those usually encountered in the domain.

68 Along the Eastern shore of the Garda lake, stratigraphic sequences pertaining to the Veneta
69 Platform Domain are outcropping (mainly constituted by limestones of shallow or extremely
70 shallow sea formation); this Platform is divided from the Lumbard Basin (mainly constituted by
71 limestone and silica deposits of open and deep sea formation) by the Ballino-Garda line: this line
72 represents the tectonic Mesozoic scarp, formed by normal or vertical faults of Jurassic-Cretaceous
73 age that significantly lowered the western sector in respect of the eastern.

74 Such tectonic line is part of a general process of relaxation that involved the whole domain starting
75 from the Late Triassic/Lower Jurassic up to the Lower Cretaceous and determined a structural
76 fragmentation of the domain in a series of structural ups and dows (block faulting, Cassinis e
77 Vercesi, 1982); this events where combined with an irregular subsidence, which controlled the
78 sedimentation characteristics. The Alpine orogeny started from the Central/Upper Cretaceous with
79 compressive tectonic which carried on in three distinct phases, interspaced by periods of tectonic
80 stasis.

81 The study area is constituted by structural elements that formed or reactivate during the last phase
82 of the Alpine orogeny, which took place from 29-25 Ma and 10-7 Ma.

83 In this zone a continuous stratigraphic sequence of sedimentary limestone units of ages between the
84 Upper Trias (Norico) and the Eocene can be recognized; frequently, however, this sequence is not
85 regular. The various Units outcropping in the study area, from the oldest to the youngest, are
86 constituted by an alternation of dolomia limestone and compact and crystalline limestones of
87 greyish-white colour (Castellarin, 1982).

3 Method of study

88

89 Rockfall phenomena are frequently recorded in coastal areas where high cliffs are present. Where
90 coastal areas are densely inhabited, an intrinsic hazard condition can become a high risk condition

91   (Fig. 1). Risk assessment is an important tool for designing mitigation measures and for planning
92   rational land use in these areas. The absolute risk assessment, however, requires analysis in terms of
93   probability of occurrence based on systematic recording of instability phenomena that are seldom
94   available. For zonation purposes, however, expressing hazard, and thus risk, in relative terms
95   (Canuti et al., 1998) is possible.

96   Many researchers have been dedicated to improve rockfall susceptibility at local and larger scale
97   (Agliardi and Crosta, 2002; Crosta and Agliardi, 2003; Jubyedoff et al., 2005; Copons and
98   Vilaplana, 2008; Frattini et al. 2008) with different aims and field of applicability: in environmental
99   mining to reduce accidents in quarries (Alejano et al., 2008), to solve rockfall problems along
100 public roads (Schweigt et al., 2003; Guzzetti et al., 2004), or to generally improve land use planning
101 (Abellán et al., 2006).

102 Many of these works outline the importance of improving forecast reliability by developing more
103 powerful modelling tools (Agliadi and Crosta, 2003; Dorren, 2003) and by a more accurate
104 geotechnical and geomechanical characterization of the slopes (Schwegh et al., 2003). The rock
105 mass structure evaluation is important for determining the detachment zones and kinds but also the
106 rock block volume and shape. The importance of a better estimation of the block features is also
107 needed to forecast the block runoff and its velocity, energy, etc. (Okura et al., 2000; Dussage et al.,
108 2002) . These results also have been validated by applying numerical and physical models based on
109 a series of probabilistic analysis to take rock mass variability into account and on in situ tests (Giani
110 et al., 2004).

111 This paper presents the application of an hazard and risk zonation methodology called Rockfall
112 Hazard Assessment Procedure (RHAP) (Mazzoccola and Sciesa, 2001) based on an aerial
113 photogrammetrical survey done by helicopter and elaborated to obtain both slope geometry and
114 geomechanical information. Due to the extremely large slope dimensions (1500 m wide and 500 m
115 tall), a special noncontact procedure based on aerial photogrammetry was needed for a more
116 detailed and precise rock mass characterization.

117 A geostructural survey devoted to a systematic and quantitative description of rock discontinuities
118 is a fundamental part of the study of the stability conditions of a rock mass. Traditionally, surveys
119 were performed with a geological compass, measuring dip and dip direction directly on the
120 discontinuity. This method was difficult because discontinuities or even rock faces themselves
121 cannot be easily accessed, and the dimension is so large that data acquisition on site would have
122 been long and expensive.

123 An alternative to traditional surveys, in many cases capable of overcoming these problems, is to
124 derive dip and dip direction, as well as the location of the discontinuities, from a highly detailed
125 topographic survey—i.e., by measuring a dense "point cloud" on the rock surface. If a set of points
126 surveyed on a particular discontinuity is selected, dip and dip direction can be computed directly
127 from the equation of the best fitting plane. Therefore, the survey will provide not only the slope
128 topography but also the identification of the discontinuities in terms of position on the slope and
129 orientation, spacing, persistence, and joint hierarchy.

130 To obtain the required results, interactive or automated software tools are necessary to allow the
131 efficient selection from the point clouds of the discontinuities. The software utilized in this work is
132 based on the RANSAC algorithm (Fisher and Bolles, 1981) that allows the semiautomatic
133 segmentation of a point cloud to extract the discontinuities of a rock slope; the algorithm is
134 implemented in an interactive software program that takes a point cloud input as well as oriented
135 images. By contouring on the image, an area with one or several discontinuities, their position, dip,
136 dip direction are automatically computed (Ferrero et al., 2009).

137 Once the topography of the slope and the geostructure are known, a kinematic analysis can be
138 obtained. Among other factors, the blocky nature of the rock mass strongly influences the stability
139 conditions of the slope; consequently, a method such as the key block method, which takes the
140 discontinuities into account, is applied. The block paths are then computed by applying the
141 Colorado Rockfall Simulation Program (CRSP) code (Pfeiffer and Bowen, 1989), which determines
142 the rock block path on the basis of the lumped mass assumption (the block is considered as a mass
143 point) in a statistical manner by simulating several different scenarios for each section.

144 **4   Hazard and risk assessment**

145 The RHAP expeditious method of hazard evaluation allows for the zonation of the territory on a
146 detailed scale, referring to restricted and clearly defined classification of hazard and relative risk.
147 The extrapolation from hazard to risk has been presented in a simplified manner, as the priority of
148 the study has concentrated on hazard definition because of its complexity. The hazard zonation
149 resulting from the application of such procedures is related strictly to the investigated site and is not
150 comparable with other sites. The reason for this is that each investigated site is divided into areas
151 ranging from low to high hazard levels, independently from the absolute hazard values.

152 A rigorous hazard evaluation should consider the intensity of the phenomenon, which in turn is
153 related to the volume of the involved blocks, the traveling velocity and the probability that the event
154 should again be evaluated on the basis of a case history of the events in order to define their
155 recurrence. Often this is not practicable in an expeditious methodology, and for this reason only

156 semiquantitative parameters (block volume and shape, travelling velocity) have been chosen for
157 zonation.

4.1   Rockfall hazard zonation

159 The RHAP procedure adopted, has been suggested by the competent local authority (Lombardia
160 region) responsible of the land security and it represents an evolution of the Rockfall hazard Rating
161 System (RHRS) developed by the US Transportation Research Board. Both the method are
162 applicable when the fall involves single block having a maximum volume of 1000 m^3 and are
163 composed of several phases. A complete description of the methods is given by Pierson et al (1990)
164 and Mazzocola and Sciesa (2001). In the following, the main features of the RHAP method are
165 reported for an easier understanding of the work.

166 The first step is dedicated to the identification of rock-slope sectors with potential rockfalls.
167 Following this identification, a delimitation of homogeneous areas (Fig. 2) is carried out on the
168 basis of the geomechanical characteristics of the rock mass, of the slope morphology, and of the
169 presence of defensive systems. These features are then used for the numerical modeling of the
170 phenomenon.

171 For each homogeneous area so defined, one or more descent trajectories are chosen on the basis of
172 observation of the topographic map for the site (15 sections reported in Fig. 2). Along such
173 trajectories the numerical simulations are performed using stochastic models integrating
174 geomechanical surveys and observation of the debris accumulations at the slope toe.

175 The rockfall numerical simulation (by means of kinematic and/or dynamic models) should be
176 performed in consideration of the block-detachment zone: the block volume, evaluated using the
177 geomechanical surveys. The block shape and the restitution and roughness coefficients of the slope
178 are also considered: these should be evaluated through a detailed survey of the rockfall trajectories.

179 As this analysis has an important statistical content, performing several rockfall simulations to
180 decrease the bias is necessary. On the bases of the rockfall numerical analysis results, a preliminary
181 longitudinal zonation of the rockfall trajectories should be done, dividing the entire path into three
182 different zones:

183   (i) transit and stopping of 70% of the blocks;

184   (ii) stopping of 95% of the blocks; and

185   (iii)stopping of 100% of the blocks.

186   These percentages should be evaluated on the total amount of the simulations that were carried out,
187   along each trajectory, on the modal blocks of every considered shape, considering the most
188   unfavorable longitudinal zonation. The relative hazard classes — (a), (b), (c) — are assigned to
189   these zones which are related to rate 4, 3 and 2, respectively. In addition, in this preliminary
190   zonation, an area limited by the block's maximum traveled distance is also delimited and assigned a
191   low hazard value of 1.

192   Subsequently, the event probability is evaluated for each of the homogeneous areas by defining the
193   block detachment propension for each sector. For this purpose, the rock front must be subdivided
194   using a square net with dimensions of 20 m (Fig. 3), determined on the base of the geomechanical
195   complexity of the homogeneous area and the rock-front extension.

196   Subsequently, the number of the following 5 instability elements were observed: fracture apertures,
197   block tilting, fracture intensity areas, surface weathering and water presence;. For each of N_{tot} cells
198   the number of instability elements (n_i) were determined. Then the percentage of activity was
199   determined for each homogeneous area as follow:

200
$$activity\% = \frac{5 * N_{tot}}{\sum\limits_{1}^{N_{tot}} n_i} \cdot 100$$

201   On the basis of the activity percentage, the homogeneous areas are assigned to three groups of high
202   (>70%), medium(35%÷70%), and low (<35%) relative activity. The homogeneous areas where the
203   blocks are rolling or stopping are often partially or completely overlapping; in such cases the map
204   representation should be made in such a way as to highlight those areas having higher degrees of
205   activity, placed upon others with lower degrees of activity. The final hazard zonation is obtained
206   using the values of relative hazard classes for the block transit and accumulation areas, which will
207   be increased by 1, kept equal, or reduced by 1 depending on the activity degree of the overlooking
208   rock slope. Five hazard classes are therefore defined with values increasing from H1 to H5.

209   ## 4.2 Risk zonation

210   Once the hazard has been defined, the risk assessment and zonation can be performed.

211   In order to carry out a rigorous classification of the risk, one should evaluate the vulnerability
212   through a comparison with the intensity of the phenomenon and subsequently combine it with both
213   the hazard and the economic evaluation (which would allow for the assessment of the pending
214   damage). In the particular procedure described in the previous section, the phenomenon intensity

215 has already been taken into account for the evaluation of the hazard; the risk assessment is
216 performed more easily by combining the exposed risk elements with the hazard classes.

217 **5 Topographic survey**

218 No contact topographic methods have been recently applied to improve the geostructural survey. A
219 full description of the method is given in Ferrero et al. (2009).

220 Photogrammetry delivers three-dimensional coordinates of points with predictable accuracy from
221 stereo or multiple images (i.e., from images of the same scene taken from different standpoints).
222 The accuracy of the coordinates depends on a number of factors, which must be accounted for in
223 designing the three stages of any photogrammetric survey: camera calibration, image orientation,
224 and object restitution.

225 Using feature-based image matching and structure from motion (Roncella et al., 2005; Birch, 2006),
226 tie points can be extracted and matched automatically; therefore, image orientation can be obtained
227 without any manual measurement. Orientation parameters can also be determined directly by fixing
228 a Global Positioning System (GPS) receiver, integrated with an Inertial Measurement Unit (IMU) to
229 the camera (Vallet et al., 2000); in this case, no Ground Control Point (GCP) are necessary.

230 Object restitution can be executed manually by an operator or automatically. The first option
231 exploits the ability of the operator to select the minimum number of points necessary for reliable
232 identification of a discontinuity plane. The latter option exploits the capabilities of image-matching
233 algorithms, such as least-squares matching (Grun, 1985), to compute several thousand points in
234 seconds. Camera stations and camera focal length must be chosen to ensure appropriate image
235 resolution for the object; depending on site characteristics, terrestrial or aerial photogrammetry can
236 be used relative to the precision needed. In this specific case, helicopter aerial photogrammetry was
237 used.

238 One point every 10 cm, with a precision of 5 cm, was required for all rock slopes. Six representative
239 areas of 10 m× 10 m were identified as particularly interesting from the geomechanical point of
240 view, and one point every 1–2 cm was measured. A focal length of 18 mm for a DTM (digital
241 terrain model) of 10 cm spacing and a focal length of 50 mm for detailed areas were adopted. The
242 shooting distance was about 100 m with parallel flying strips to obtain 50% of superimposition. Fig.
243 4 shows the shooting position during the flight.

244

5.1 Interactive extraction of planar surfaces with RockScan

A software package named RockScan has been developed to allow the interactive extraction of planes based on the RANSAC procedure. The user loads an oriented image of the rock slope and the point cloud in the background. Through a graphical user interface, Regions of Interest (ROI) enclosing one or more discontinuities can be selected drawing polylines in the image; the corresponding points are selected in the point cloud and input to the RANSAC. For each ROI, dip and dip direction of all the identified planes are computed.

With respect to processing parameters, with a few trials the user can adapt the acceptance threshold in RANSAC to account for measurement noise, resolution of the point cloud, and roughness of the discontinuity surface; values in the range of 5 to 20 cm were found to be appropriate in the cases given later. The discontinuity parameters are output in an appropriate format for the ensuing geometric modeling of the rock face. Figures 5 and 6 show orthophotos of the south and north cliffs, with the detailed areas shown in Fig. 7.

5.2 Geostructural survey

A geostructural survey was performed in detailed areas indicated in figures 5 and 6 by analyzing 1445 planes distributed in the six areas (Fig. 7).

Statistical evaluation of the rock-mass structure was then performed by use of the commercial code DIPS (Rockscience) to determine the joint sets in each area. Fig. 8 shows the stereogram reproduction of the isocurves of measured poles and joint sets identified in each zone.

For each detailed zone, virtual scanlines were constructed in order to measure the discontinuity spacing and relative frequency distribution, as shown in Fig. 9, that also shows exponential interpolation curves, as evidenced in the literature (Priest and Hudson, 1981). The homogeneity of two observed zones is noteworthy for joining together data belonging to the south and north slopes.

On the south slope, four detailed areas were identified: zones 1, 2, 3, and 4 in figures 5 and 7. Also, 923 planes were measured in terms of orientation and spacing. Four joint sets (K1, K2, K3, and K4) were identified, as reported in Fig.8.

On the North slope, 218 poles were measured in two detailed zones (zones 5, 6 in Figure 6 and 7) where, again, four joint sets were identified (K1, K2, K3, K4). Orientation data are reported in Tab. 1, considering that average spacing was estimated to be equal to 0.20 m, varying between 0.05 and 0.59 m. As shown in Table 1, the slopes exhibit a similar structure characterized by bedding plane (K1) and three subvertical joint sets.

6 Analysis of potential instability phenomena

The stability of the rock slopes is due mainly to the rock-mass structure. The orientation of the discontinuities in relation to that of the slope determines the kinetic potential of the rock blocks to move along the discontinuity planes or their intersections. Limit equilibrium methods (LEM) therefore can be applied to verify the stability condition of possibly unstable blocks. Among others, the key block theory can be applied to identify critical blocks as a result of discontinuity intersections in a rock mass free along defined surfaces. The critical blocks can liberate other blocks that were previously restrained, once they move or detach from the rock mass.

6.1 Key block theory

The essential part of the key block theory is the analysis of the discontinuity system in conjunction with the free surfaces. Intersecting discontinuities, these surfaces originate solids of variable shape that, in connection with either externally applied forces or mobilizable strengths, can leave free surfaces and be in critical stability conditions. The theory aims to identify the critical blocks that, in the absence of appropriate contrast, release other blocks near the digging and trigger the collapse of the rock structure. The block in the most dangerous position, the first to be released, is defined as the key block. If the potentially dangerous block (key block) is identified before movement begins, and if its stability is assured, then the other blocks will not move. The method can be implemented either with a vector calculus or a graphic process. The graphic process uses equiangular stereographic projection. This kind of projection represents a particular perspective form in which a single projection point exists, which coincides with one of the two projection sphere poles, in this case the lower pole. The assumptions on which the method is based are perfectly plane discontinuity surfaces, continuous at least inside the blocks and characterized by a definite direction beforehand; nondeformable blocks; and the possibility of movement only without interference from adjoining blocks.

The block method distinguishes "indoor" rock-mass blocks (JB) from the blocks that overlook the digging surfaces (JP). The finite blocks can be either removable or nonremovable. Removable blocks are further divided into all identical stable blocks, stable blocks thanks to shear strength on discontinuities, and unstable blocks (key blocks). To define a finite and removable block stability condition, comparing acting and reacting forces is necessary. For this purpose, applying either an analytical or a graphic procedure is possible to define friction-angle values able to maintain a stable joints pyramid in connection with a potential sliding condition.

307 The ROCK3D (Geo&Soft, 2008) program is used for the block analysis and calculus, as stated
308 previously. Using Goodman & Shi's (1985) key block theory, the calculus code recognizes possible
309 kinematic mechanisms of blocks and estimates their stability in connection with extreme
310 equilibrium. This analysis assumes that it is possible to associate a definite rock volume to every
311 kinematic mechanism (release, sliding on one or two planes), even with a complex shape or
312 bounded by different discontinuity planes and digging walls (if the discontinuity grid geometry
313 allows that).

314 For a selected kinematic mechanism the program defines (according to the discontinuity tracks
315 surveyed on the slope), the maximum close boundaries (which are not connected to each other),
316 using only discontinuities that are connected and compatible with the examined kinematic
317 mechanism. This analysis phase and the next phase must be repeated for every possible kinematic
318 mechanism, looking for the greatest instability conditions. The program optionally generates a
319 pseudorandom discontinuity map that respects the statistical distribution of frequencies and
320 persistencies measured on the natural slope. In this way making a certain number of simulations is
321 possible to anticipate the behavior of rock fronts before the on-site intervention. The next phase is
322 directed to the complete geometrical reconstruction of complex blocks. The program defines the
323 solid derived from the union of all elemental polyhedrons contained within close boundaries,
324 eventually separated, identified in the following sections. For each complex block, ROCK3D
325 calculates volumes and surfaces. The kinematic mechanism analysis, made using Goodman & Shi's
326 (1985) block theory, allows us to associate every existing kinematic mechanism (release, sliding on
327 one or two planes) and a definite rock volume, even with complex shape, if the discontinuity grid
328 geometry allows that. The analysis used in this phase is divided into three phases:

329   (i) recognition of all rock pyramids created by the intersection of families of discontinuity
330   planes;

331   (ii) recognition of rock pyramids that, in association with externally applied strengths, may
332   possibly move; and

333   (iii) recognition of the removable blocks in connection with the previous ones that, according to
334   their position, may be in critical stability conditions.

6.2 Results

336 The application of the key block theory in this work has determined the following results. The rock
337 slope has been divided into six detailed areas and in two domains (northern front and southern

338 slope), according to the results of in situ surveys as reported in the previous chapter. The space
339 pyramid projections obtained in the two domains are reported in Fig. 10 for all the analyzed areas.

340 In all analyzed areas, the most common kinematic is determined by the intersection between two
341 subvertical joint sets, K2 and K4 (in some cases K3 can replace K4, isolating similarly shaped
342 blocks), and at the base cut by bedding plane (K1). Those blocks are denominated key blocks as
343 100, in other words under discontinuity K1 and above K2 and K3, as shown in Fig. 11. The same
344 figure also shows, depending on the inclination of the intersection line between K2 and K4, that
345 owing to verticality the block could plunge downhill or uphill and that it could slide on the
346 intersection line or topple. The described phenomena can be observed in several cases on the slope.

347 Other kinds of removable blocks are determined by the key block method, but their JP are
348 completely within the reference circle, indicating that their movement direction could only have
349 been upward and, consequently, that instability could not occur under pure gravity.

350 Finally, one could observe that if weathering effects occur on the bedding planes, the movement of
351 other block types could be determined by different key block types, which should be considered in
352 the design of mitigation measurements.

353 Table 2 reports the block types computed for the six areas. Where the numbers 0 and 1 represent the
354 block position below or above the discontinuity respectively. Block dimension is strongly
355 influenced by spacing that averages between 10 and 25 cm, with maximum values of 50–60 cm.

356 **7 Rockfall analysis**

357 For the bidimensional analysis of the motion of single blocks traveling downslope, the calculation
358 methodology proposed by Pfeiffer and Bowen (1989), who introduced it in the numerical code
359 CRSP, has been chosen. This numerical program was developed in 1989 at the Colorado School of
360 Mines, Department of Geology and Geological Engineering, in collaboration with the Colorado
361 Department of Highways. The CRSP code was based on the experiences of various authors
362 (Ritchie, 1963; Piteau and Clayton, 1977) and was calibrated using several experimental results
363 obtained from artificially induced rockfalls along unstable slopes located in West Rifle and the
364 Colorado Canyons (Colorado, USA).

365 In order to describe the block movement along the slope, the numerical code applies the equation of
366 the parabolic motion of a free-falling mass and the principle of total energy conservation. The
367 analysis is carried out dynamically, as the motion parameters calculated at one step are applied to
368 the following step and as the combined effects of free falling, rebound, rolling, and sliding are taken
369 into account as well.

370   The analysis of the Campione del Garda slope has been performed along 15 different sections (Fig.
371   2). The sections have been carefully chosen by the analysis of the morphology of the territory. For
372   each section, 500 numerical simulations have been performed; and a statistical analysis of the
373   results has been applied in order to calculate the modal values of kinetic energy, rebound height,
374   and travel length of the blocks (Fig. 12).

375   The starting point for the rockfall has been chosen conventionally as the highest point of each
376   section. The restitution coefficients Kn e Kt (Giani, 1997) used for the rockfall analysis were
377   assumed as follow:

378   • outcropping rock: Kn = 0.3 and Kt = 0.8 with a standard deviation (s.d.) of 0.02, and friction
379   angle (ϕ) equal to 30° (s.d. of 2°);

380   • debris areas covered by vegetation: Kn = 0.2 and Kt = 0.4, (s.d. of 0.02), and friction angle
381   (ϕ) equal to 40° (s.d. of 2°);

382   • debris areas without vegetation: Kn = 0.3 and Kt = 0.6 (s.d. of 0.02), and friction angle (ϕ)
383   equal to 35° (s.d. of 2°).

384   The phenomenological features have been calibrated on the basis of the observation of the blocks
385   surveyed at the slope foot.

386   The coordinates of the lines forming the slope profile and the restitution and roughness coefficients
387   associated with each portion of the block path have been indicated in the input files. The starting
388   horizontal and vertical velocities, computed on the base of detachments conditions, have been
389   constantly assumed to be equal to 1 and 0.5 m/s. The block shape has been considered spherical,
390   with a recurring diameter of 0.3 m for what is considered to be the traveled path (the 0.3 m diameter
391   causes the longest path and therefore the widest hazard zones). For the kinetic energy calculation,
392   the block that produced the least favorable results (i.e., the higher energy) was spherical with a 0.5
393   m diameter.

394   For each section, the velocities, rebound heights, and maximum, average, and minimum kinetic
395   energies have been calculated; the cumulative probability distributions of the velocities, kinetic
396   energies, and rebound heights have been drawn for each part of the slope section. The number of
397   blocks that stop at each slope progressively have also been recorded (Fig. 13).

398   For each homogeneous area of the slope front, the predisposition to block detachment has been
399   defined as well. The activity value (considering the five parameters indicated by the adopted
400   methodology, RHAP), the total possible unstable elements, and the relative activity (computed by
401   comparing different cell activity of the same slope) have been determined for each investigated cell.

402   The activity value is considered low when <35%, medium between 35% and 60%, and high >60%.

403   These degrees of activity, determined for the three different areas, resulted in 64%, 61%, and 64%,

404   respectively, characterizing the whole front as being of "high" activity.

405   The hazard zonation has been obtained using the values of the hazard classes, determined on the

406   basis of block arrest and transit percentages, increased by 1 as the activity of the front classified as

407   "high." (Fig. 14).

408   ## 7.1   Mitigation measures

409   Several defensive systems were evaluated in order to reduce the hazard zones on the basis of the

410   accomplished results. Various typologies have been examined. Those that would better fit the area

411   are described below. For this purpose the whole town of Campione del Garda has been divided the

412   following several sectors (Fig. 15):

413   (i) *northern zone, Gardesana tunnel exit*: the existing tunnel should be lengthened at least 50

414   m outside the rock front and should be covered with 1 m of debris. The tunnel should be

415   designed to face impacts of 600 kJ of energy. The rock block for the design should be

416   considered spherical with a 0.5 m diameter as observed in situ;

417   (ii) *northern zone, embankment area*: the embankment, 4.5 m high, should be placed along

418   the side of the rock front, protecting the Gardesana State Road. This embankment should

419   begin directly at the side of the tunnel exit and should cover the whole area subjected to

420   the risk. The area behind the embankment should be prohibited to people, and the ground

421   should be ploughed for the first 0.5–1 m in order to soften it and increase its energy

422   absorption capacity. The maximum energy for impact on the embankment should be

423   considered equal to 250 kJ;

424   (iii) *central zone, cemetery proximity*: this area is the most difficult to protect, owing to the

425   presence of structures in close proximity to the rock front and directly reachable by falling

426   blocks (cumulative probability of about 50%). The installation of high-energy-absorption

427   rockfall barriers allows for a reduction of the rockfall-induced risk. The maximum impact

428   energy is equal to 1000 kJ, and the barrier height should be equal to 5 m;

429   (iv) *central and southern zones, between the cemetery area and the southern tunnel:* this area

430   should be protected with an embankment 6 m high, which should be placed along the

431   front edge of the rock, protecting a road. This embankment should begin directly adjacent

432   to the southern tunnel entrance and cover the whole area subjected to rockfall-induced

433   risk. The area behind the embankment should be prohibited to people, and the vegetation

434 should be preserved because it helps in the reduction of impact energy. The maximum
435 impact energy calculated for the embankment is equal to 250 kJ; and

436 *(v) southern zone, tunnel entrance:* the existing tunnel (the northern tunnel) should be
437 lengthened to at least 30 m and should be covered with at least 1 m of debris. The impact
438 energy calculated for the top of the tunnel is equal to 600 kJ. The shape of the design
439 block should be considered spherical with a 0.6 m diameter as observed in situ.

440 A two-dimensional rockfall analysis by using CRSP code was performed that took into account the
441 presence of the above-described protection systems. A new final hazard zonation was then
442 calculated and is shown in Fig. 15, where reduction of the high hazard zone can be seen.

7.2 Monitoring systems

444 During the geomechanical survey of the cliffs overlooking the town of Campione del Garda, a few
445 potentially unstable blocks of considerable dimensions were observed.

446 These blocks are beyond the scope of this study, as their fall would most probably trigger a wider
447 rockslide. Owing to the dimensions of those blocks, any passive defensive system would not be
448 economically practicable. Nevertheless, monitoring the stability of such blocks should be
449 considered absolutely essential for the safety and protection of the Campione del Garda inhabitants
450 and structures. Thus, in order to design an appropriate monitoring system, further studies should be
451 undertaken.

8 Conclusions

453 The Campione del Garda coastal cliff area is subject to high hazard and risk owing to rockfall
454 phenomena. This situation needs to be mitigated by proper defensive and reinforcing methods for
455 protection of the inhabitants and the structures. The design of the mitigation interventions must be
456 based on the area's risk zonation in order to identify the optimum systems and locations.

457 The assessment of absolute risk should be based on historical data and occurrences of these
458 phenomena, which are not available for this area. Consequently, a relative hazard evaluation based
459 on the RHAP and adopted by several Italian institutions has been chosen. A kinematic analysis
460 based on rock-mass structure has been performed to compute the probability of block detections on
461 the slopes. This analysis was conducted by applying the key block method, which allows
462 identification of the types of possible instability and evaluation of the block volumes. A block-path
463 probabilistic analysis was then performed on several potentially hazardous sections and a two-
464 dimensional analysis was made using the CRSP method.

465 Zonation of the relative hazard indicated mitigation measures that need to be adopted: artificial
466 gallery accessing road protections, walls to avoid access to high hazard areas, removal of unstable
467 blocks and monitoring of possible zones of unstable slopes. Designs of these various measures
468 could be based upon the quoted lumped mass analysis in terms of impact energy to be absorbed (for
469 the gallery and the walls) and for the definition of the structural dimensions (e.g., the gallery
470 lengths). A new hazard zonation was completed in consideration of the proposed mitigation
471 measures for quantifying the final hazard potential for the coastal cliff.

472 9 References

473 Abellán, A., Vilaplana, J.M., Martínez J., 2006. Application of a long-range terrestrial laser scanner
474 to a detailed rockfall study at Vall de Núria (eastern Pyrenees, Spain). Engineering Geology, 88,
475 136–148.

476 Agliardi, F., Crosta, G., 2003. High resolution three-dimensional numerical modelling of rockfalls.
477 International Journal of Rock Mechanics and Minining Science, 40(4), pp. 455–471.

478 Alejano, L.R., Stockhausen, H.W., Bastante, F.G., Alonso, E., Ramíez-Oyanguren, P., 2008.
479 ROFRAQ: an empirical method to estimate the risk of accidents due to rockfalls in quarries.
480 International Journal of Rock Mechanics and Minining Science, 45(8), pp.1252–1272.

481 Birch, J., 2006. Using 3DM analyst mine mapping suite for rock face characterization. In Tonon, F.,
482 Kottenstette, J. (Eds.). 41st U.S. Rock Mechanics (ARMA) Symposium Laser and Photogrammetric
483 Methods for Rock Face Characterization. Golden, Colorado (USA). pp. 13-32.

484 Canuti, P., Casagli, N., Tarchiani, U., 1998. Rock fall hazard in coastal cliffs. Proceedings of 8th
485 IAEG Congress, Vancouver,. Balkema Ed., Rotterdam, The Netherlands, pp. 1585–1592

486 Cassinis, G., Vercesi, P.L., 1982 - Lineamenti strutturali fra la Val Trompia e la Val Sabbia
487 (Brescia) durante il tardo Trias ed il Giurassico inferiore. Boll. Soc. Geol. It., 101, pp. 317-326.

488 Castellarin, A., 1982. Lineamenti ancestrali sudalpini. In Castellarin, A., Vai, G.B. (Eds.): Guida
489 alla Geologia del Sudalpino centro-orientale. S.G.I., Guide Geol. Reg., pp. 41-55.

490 Crosta, G.B., Agliardi, F., 2003. A new methodology for physically based rockfall hazard
491 assessment. Natural Hazards Earth System Science, 3(5), pp. 407–422.

492 Dorren, L.K.A., 2003. A review of rockfall mechanics and modelling approaches. Proceeding in
493 Physical Geography, 27 (1), pp. 69–87.

494 Dussauge, C., Helmstetter, A., Grasso, J.R., Hantz, D., Desvarreux, P., Jeannin, M., Giraud, A.,
495 2002. Probabilistic approach to rock fall hazard assessment: potential of historical data analysis.
496 Natural Hazards Earth System Science 2, pp. 15–26.

497 Ferrero, A.M., Forlani, G.F., Roncella R., Voyat, H.I., 2009. Advanced Geostructural Survey
498 Methods Applied to Rock Mass Characterization. Rock Mechanics and Rock Engineering, 42(4),
499 pp. 631-665.

500 Fisher, M., Bolles, R., 1981. Random Sample Consensus: A paradigm for model fitting with
501 application to image analysis and automated cartography. Communication of the ACM, 24 (6), pp.
502 381–395.

503 Frattini, P., Crosta, G., Carrara, A., Agliardi, F., 2008. Assessment of rockfall susceptibility by
504 integrating statistical and physically-based approaches. Geomorphology, 94 (3-4), pp. 419–437.

505 Geo&Soft., 2008. Key Block Theory Based on Three-Dimensional Rock Block Analysis. Rock3D.
506 Manual. Available online in: http://www.geoandsoft.com.

507 Giani, G., 1997. Caduta massi: Analisi del moto ed opere di protezione. Ed. Hevelius, Benevento,
508 Italy, 120 pp.

509 Giani, G.P., Giacomini, A., Migliazza, M., Segalini, A., 2004. Experimental and theoretical studies
510 to improve rockfall analysis and protection work design. Rock Mechanics and Rock Engineering,
511 37(5), pp. 369–89.

512 Goodman, R.E., Shi, G.H., 1985. Block Theory and its Application to Rock Engineering. Ed.
513 Prentice Hall,Englewood Cliffs, NJ, 338 pp.

514 Grun, A., 1985. Adaptive least squares correlations: a powerful image matching technique. South
515 African Journal of Photogrammetry, Remote Sensing and Cartography, 14 (3), pp. 175–187.

516 Guzzetti, F., Reichenbach, P., Ghigi, S., 2004. Rockfall hazard and risk assessment along a
517 transportation corridor in the Nera Valley, central Italy. Environmental Management, 34(2), pp.
518 191–208.

519 Jaboyedoff, M., Dudt, J.P., Labiouse, V., 2005. An attempt to refine rockfall hazard zoning based
520 on the kinetic energy, frequency, and fragmentation degree. Natural Hazards Earth System Science
521 5(5), pp. 621–632

522 Mazzoccola, D., Sciesa, E., 2001. La metodologia RHAP (Rockfall Hazard Assessment Procedure).
523 Prevenzione dei fenomeni di instabilità delle pareti rocciose. Programme Interreg II C, pp. 84-95.

524 Okura, Y., Kitahara, H., Sammori, T., Kawanami, A., 2000. The effects of rockfall volume on
525 runout distance. Engeeniring Geology 58(2), pp. 109–124.

526 Pfeiffer, T., Bowen, T., 1989. Colorado Rockfall Simulation Program. Boulder, Colorado (USA):
527 Colorado School of Mines–U.S. Dept. of Transportation, Federal Highway Administration.

528 Pierson, L., Davis, S., van Vickle, R., 1993. The Rockfall Hazard Rating System Implementation
529 Manual. Washington, USA: Oregon State Highway Division, Report FHWA-OR-90-01. Available
530 online: http://tris.trb.org/view.aspx?id=459774

531 Piteau, D., Clayton, R., 1977. Discussion of paper "Computerized design of rock slope using
532 interactive graphics for the input and output of geometrical data" by Cundall et al. Proceedings 16th
533 Symposium on Rock Mechanics, ASCE, Minneapolis (USA), pp. 62-63.

534 Priest, S., Hudson, J., 1981. Estimation of discontinuity spacing and trace length using scanline
535 surveys. International Journal of Rock Mechanics, Mining Sciences and Geomechanics Abstracts,
536 18(3), pp. 183–197.

537   Ritchie, A., 1963. Evaluation of rockfall and its control. Highway Research Record, National
538   Research Council Washington D.C, no. 17, pp 13-28.

539   Roncella, R., Forlani, G., Remondino, F, 2005. Photogrammetry for geological applications:
540   Automatic retrieval of discontinuity orientation in rock slopes. Videometrics IX—Electronic
541   Imaging—IS&T/SPIE 17th Annual Symposium, pp. 17–27.

542   Schweigl, J., Ferretti, C., Nossing, L., 2003. Geotechnical characterization and rockfall simulation
543   of a slope: a practical case study from south Tyrol (Italy). Engineering Geology, 67(3-4), pp. 281–
544   296.

545   Vallet, J., Skaloud, J., Koelbl, O., Merminod, B., 2000. Development of a helicopter-based
546   integrated system for avalanche and hazard management. Int. Archives of Photogrammetry and
547   Remote Sensing, pp. 565–572.

Figure

Fig. 1. View of the Campione del Garda inhabited shore on the western coast of Lake Garda (Northern Italy).

Figure

HOMOGENEOUS
AREA

Area 1
Area 2
Area 3

Vertical Section for
Rockfall analyses
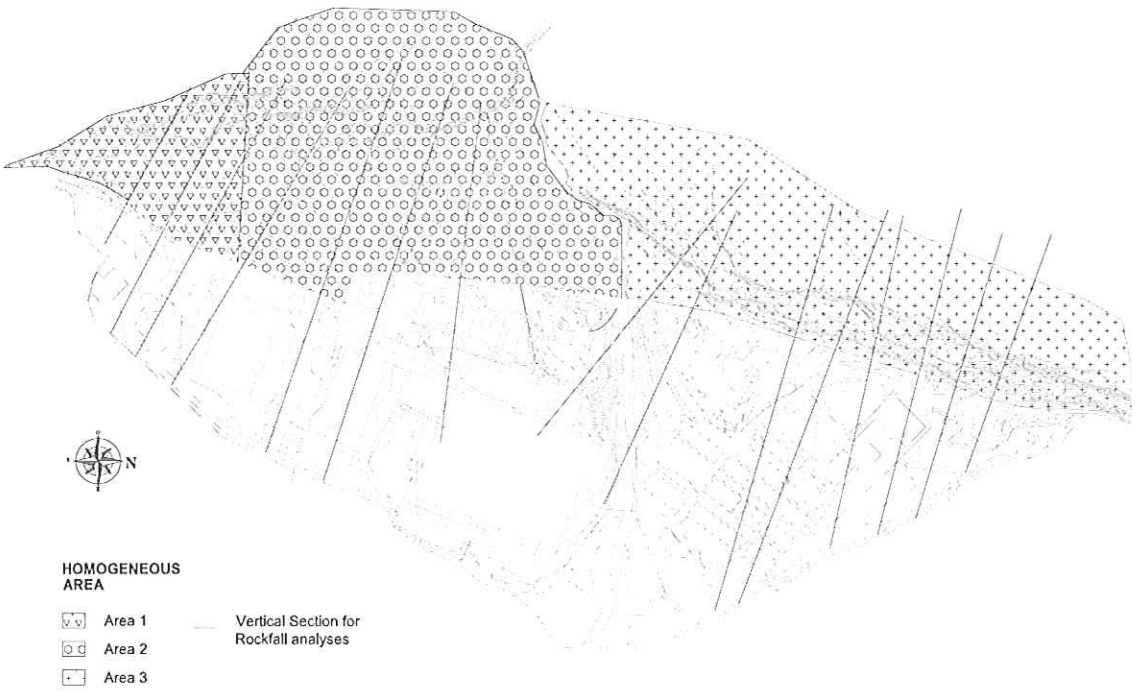
Fig.2. Definition of homogeneous areas on the base of the geomechanical characteristics of rock mass and traces of vertical sections utilized for rockfall analyses.

Figure
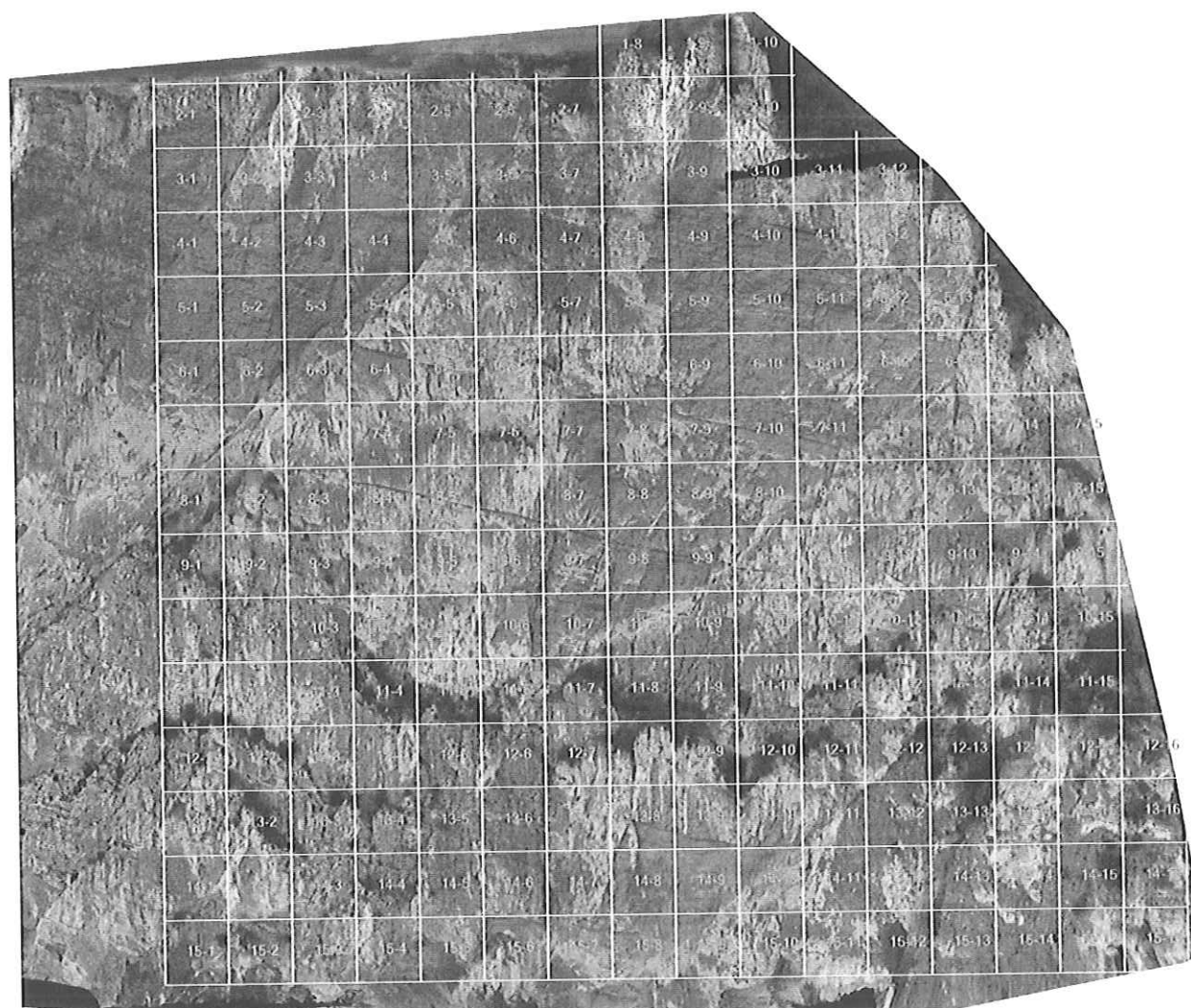
Fig. 3. Northern slope: square net utilized for the determination of the number of instability elements in the rockfall hazard zonation procedure.

Figure
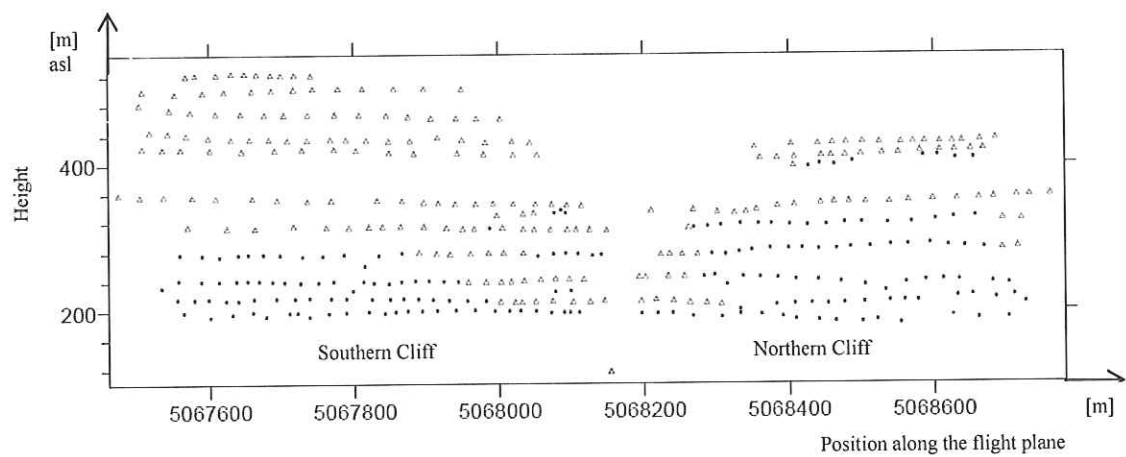
Fig.4. Shooting position during helicopter flight.
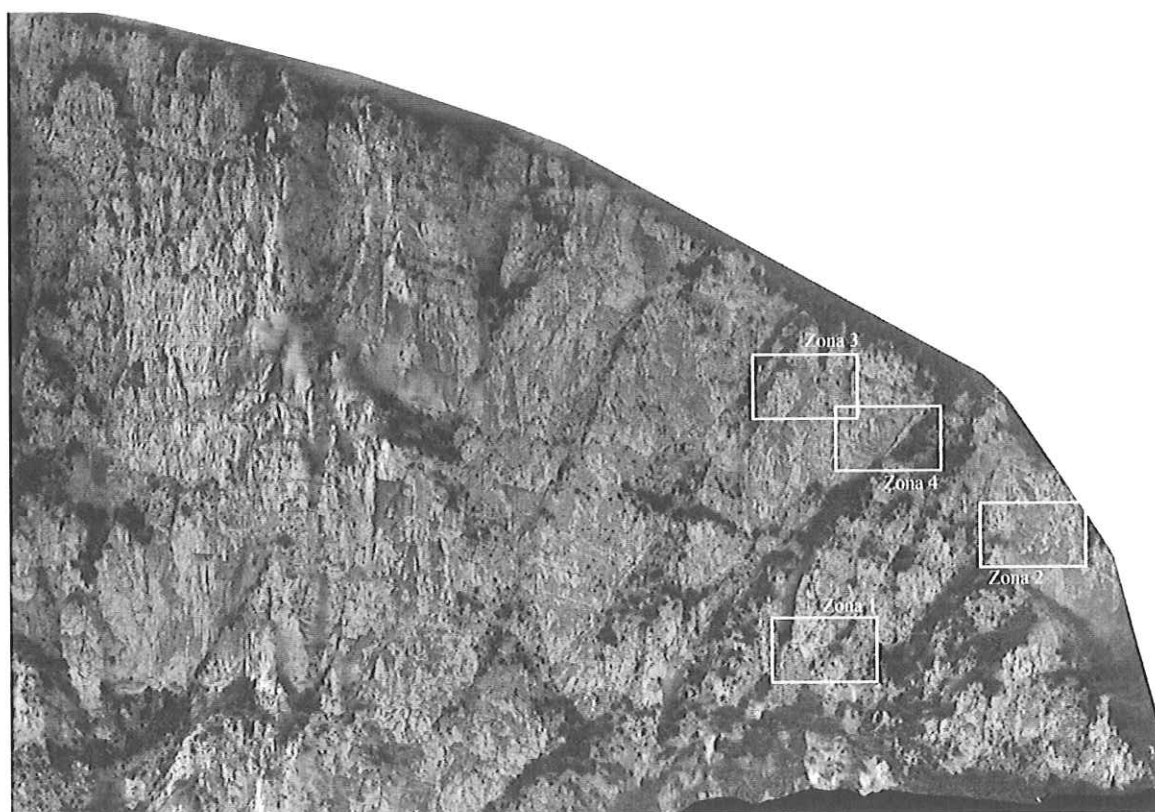
Figure

Fig. 5: South cliff orthophoto with indication of detailed areas.
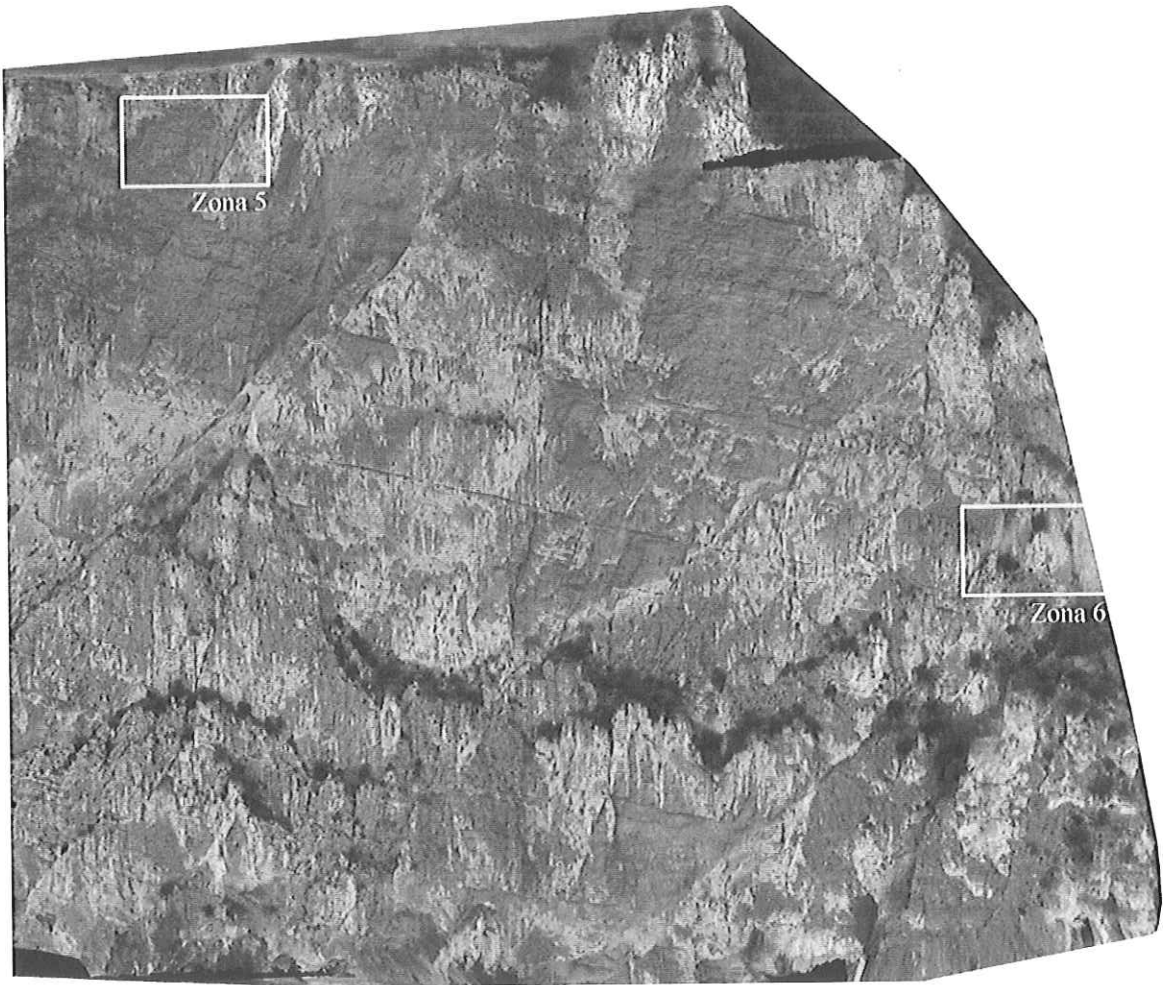
Fig. 6: North cliff orthophoto with indication of detailed areas.

Figure

Zone 1

Zone 2

Zone 3

Zone 4

Zone 5

Zone 6
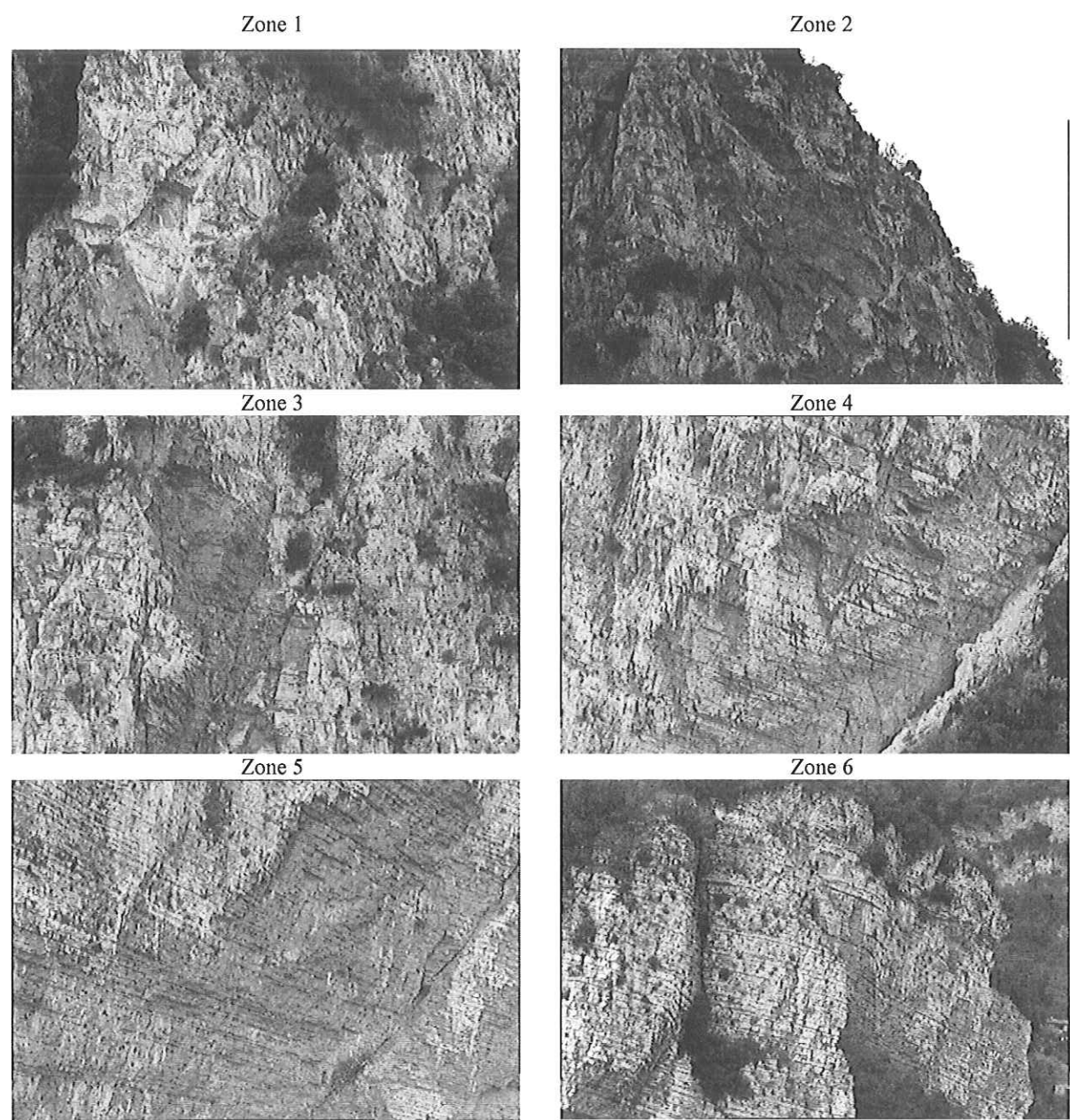
Fig. 7: Zones of detailed survey. Main Dolomite outcrop where apparent are the bedding strata and some vertical joints.

Figure
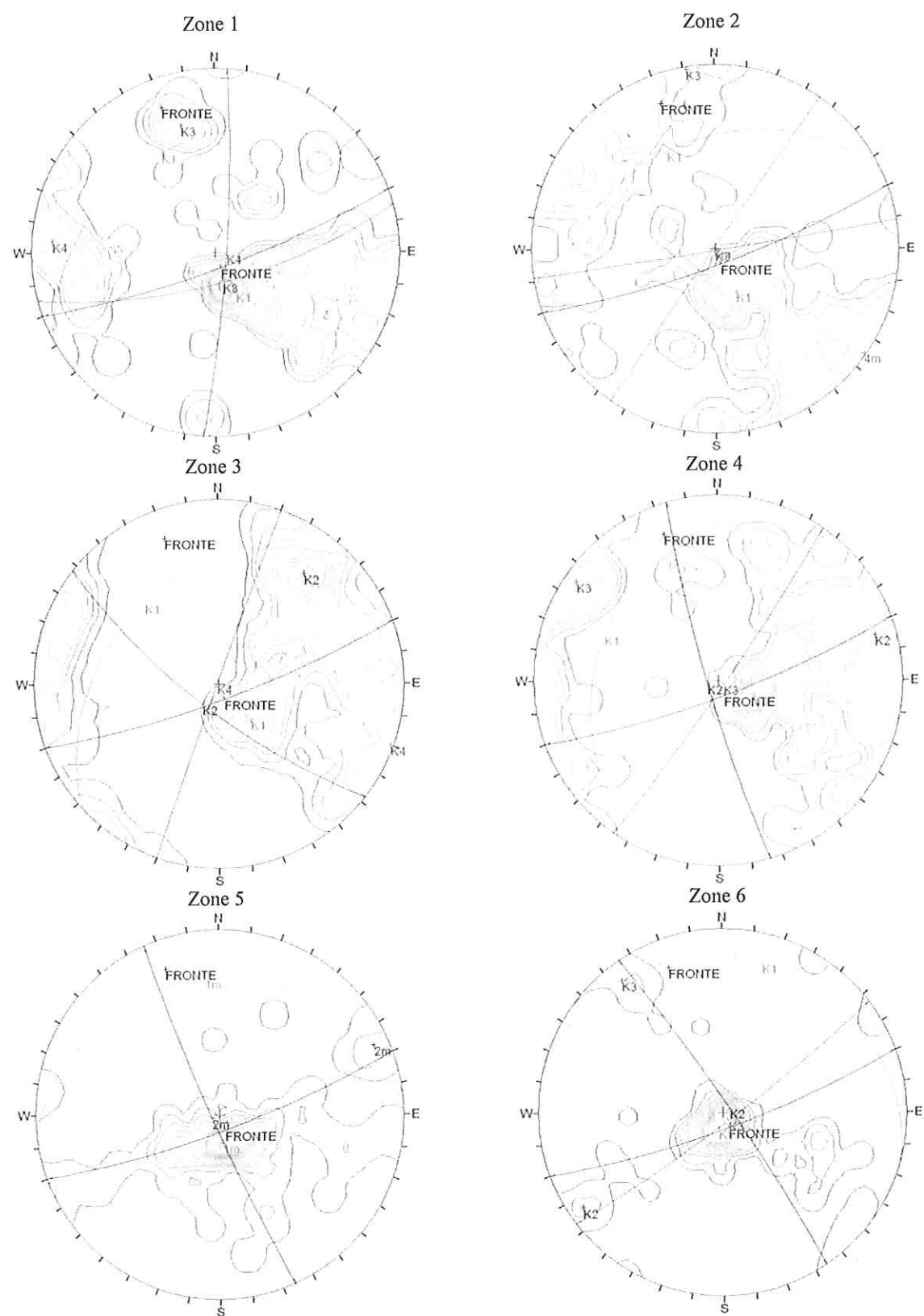
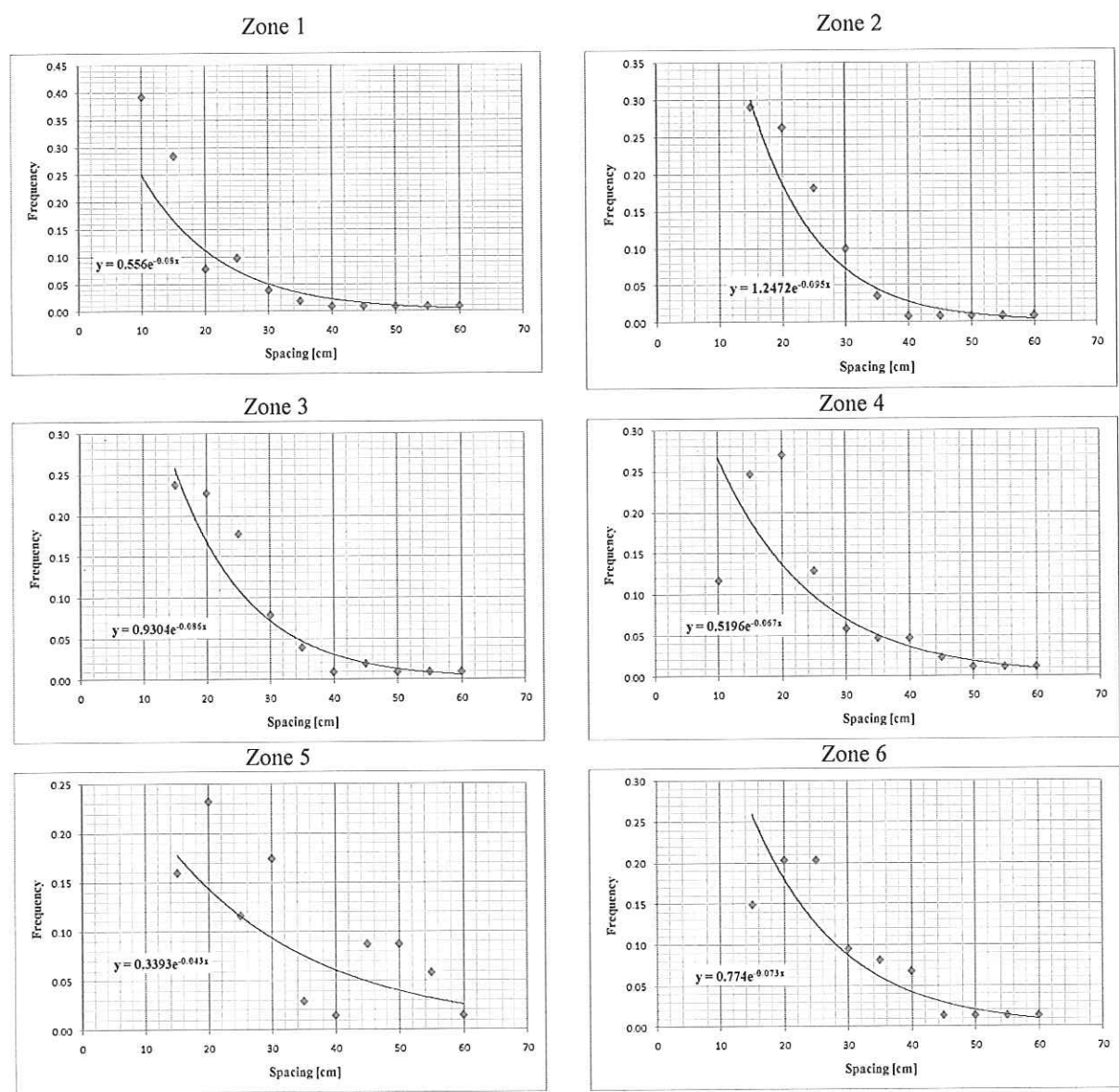Fig. 8: Stereogram reproduction of the isocurves of measured poles and joint sets identified in each zone.

Figure

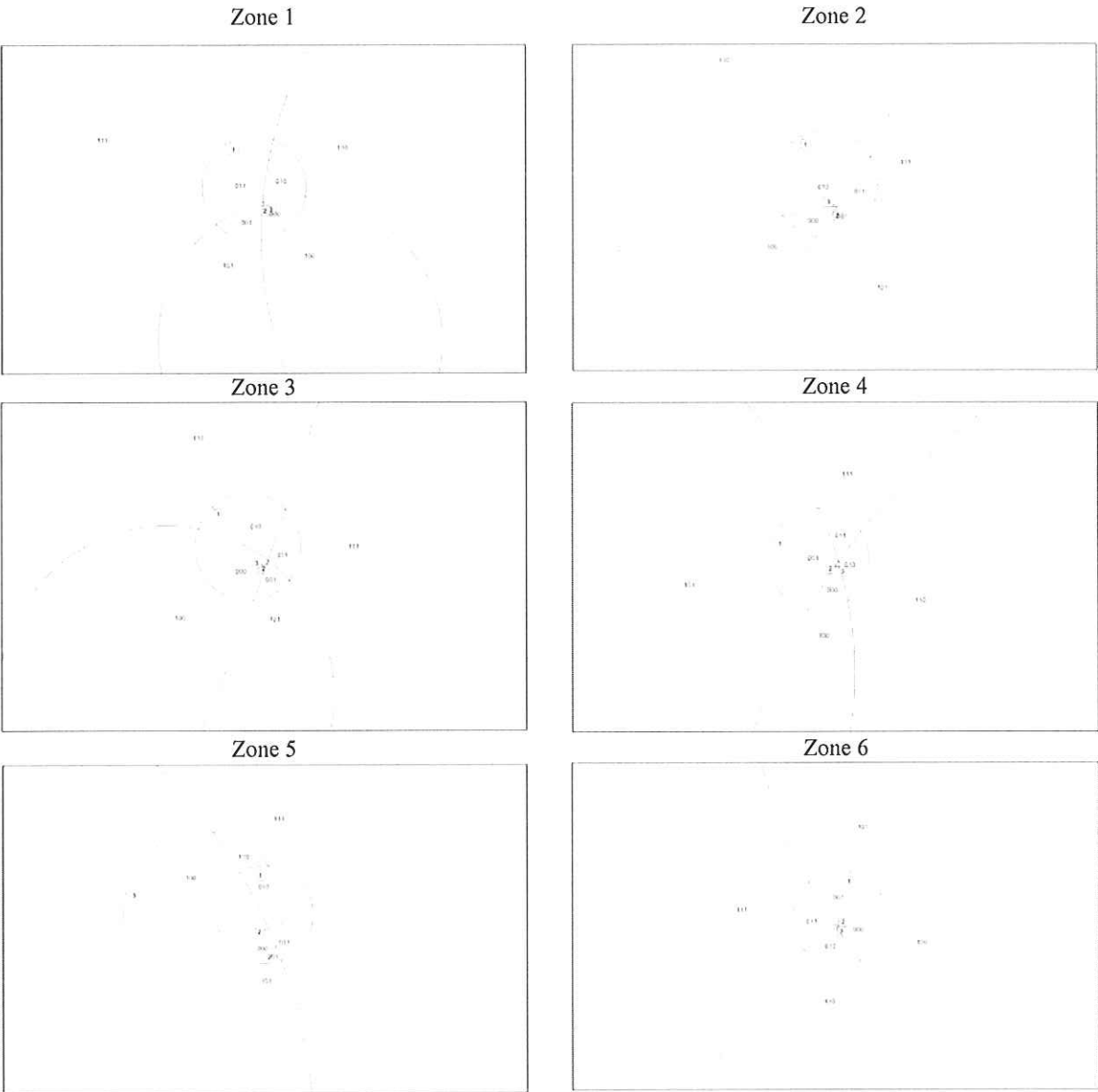Fig. 9: Spacing distribution measured in each detailed zone.

Figure

Zone 1

Zone 2

Zone 3

Zone 4

Zone 5

Zone 6

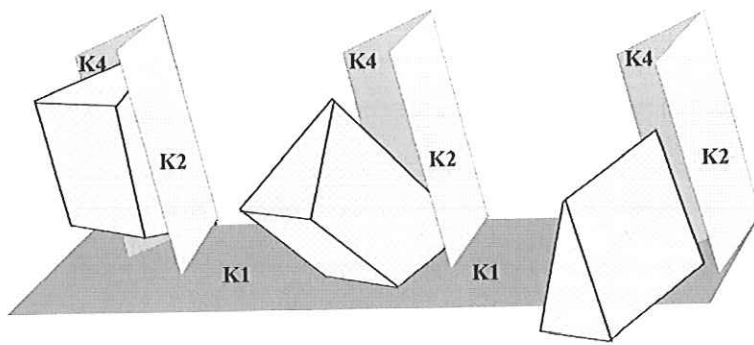Fig. 10. Space pyramid projections computed in the six analyzed areas.

Figure

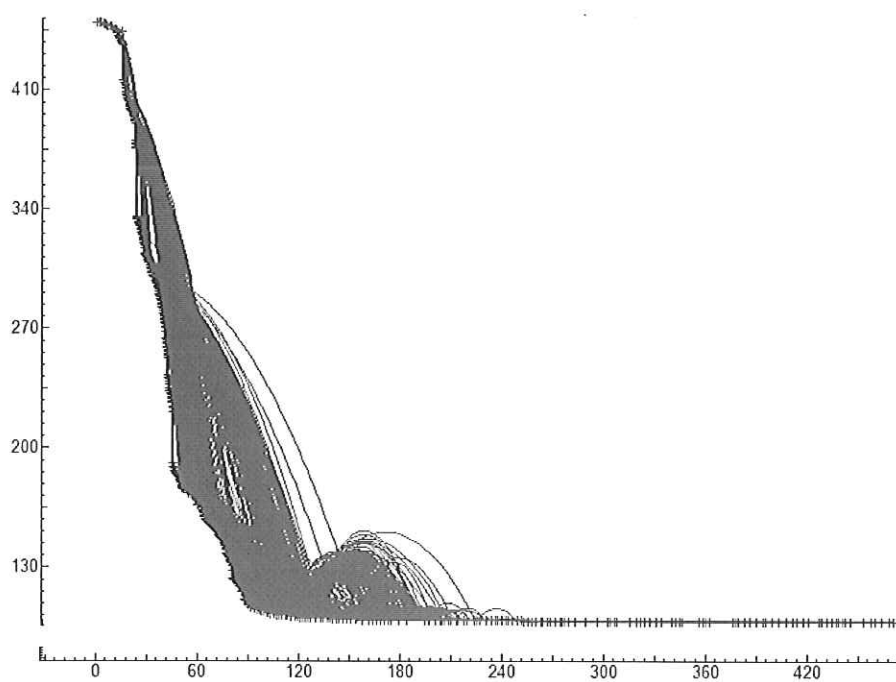Fig.11. Schemes of computed instability phenomena.

Figure

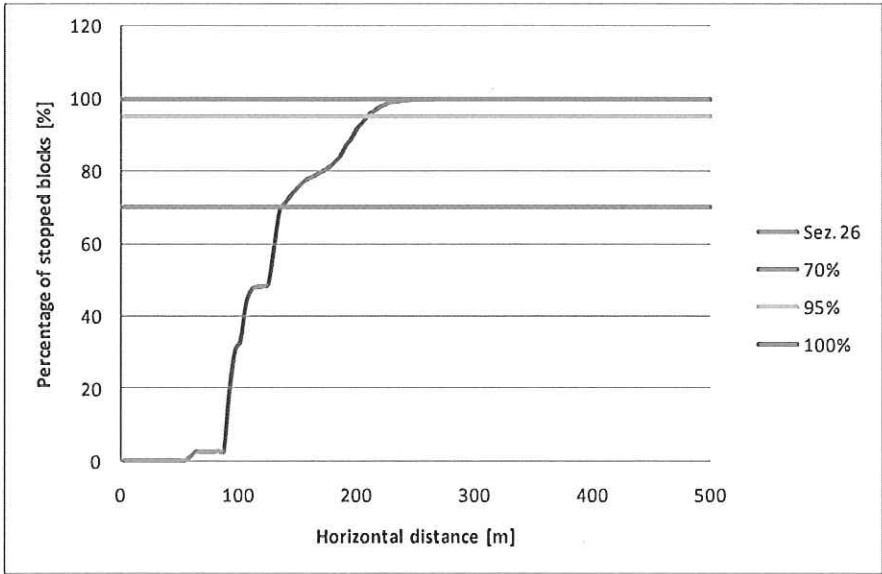Fig. 12. Indication of the 500 analyzed paths in one analyzed section.

Figure

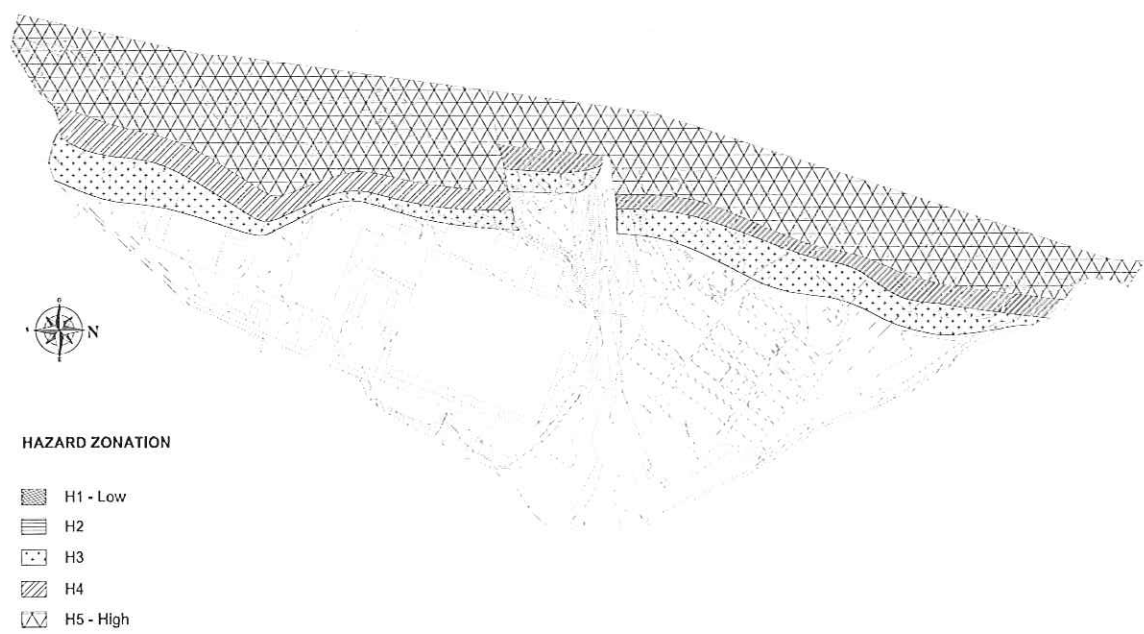Fig. 13. Cumulative frequency of arrested block distance.

Figure

HAZARD ZONATION

▨ H1 - Low
▤ H2
▦ H3
▨ H4
▨ H5 - High

Fig. 14.Preliminary hazard zonation map. The lines indicate the 15 vertical sections along which rockfall were analyzed.

Figure

HAZARD ZONATION

- ▨ H1 - Low
- ▤ H2
- ⬚ H3
- ▨ H4
- ▽ H5 - High

MITIGATION MEASURES

- ■ Rockfall defensive tunnel
- ☐ Reinforced earth embankment (H = 4.50 m)
- ☐ Reinforced earth embankment (H = 6.0 m)
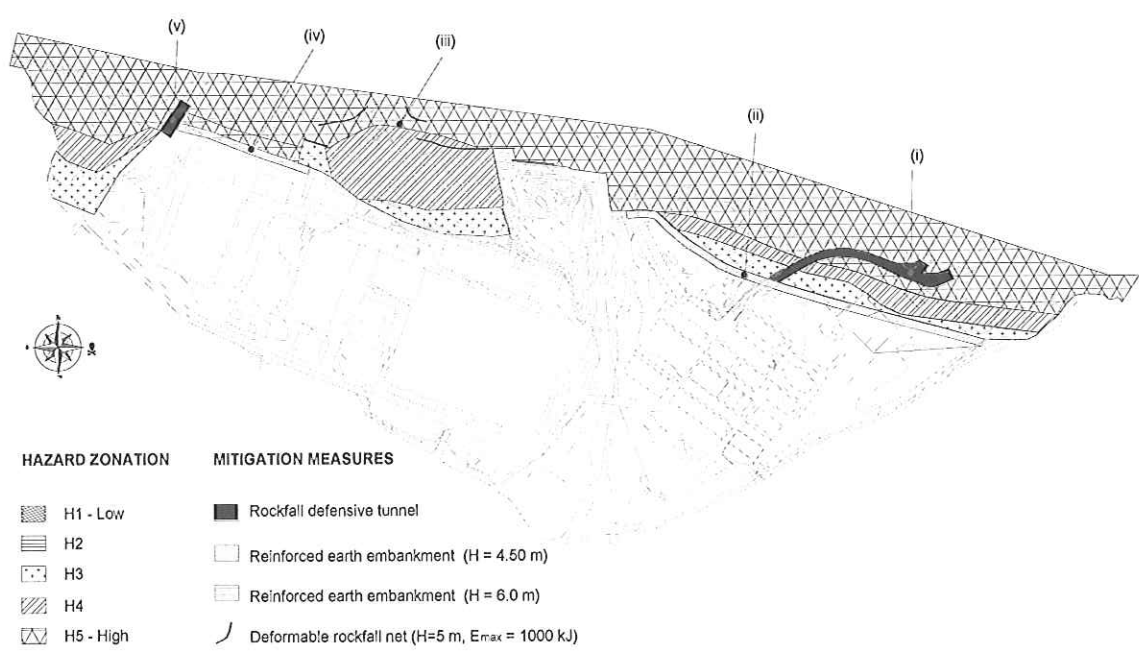- ⌐ Deformable rockfall net (H=5 m, E_{max} = 1000 kJ)

Fig. 15. Final hazard zonation map and indication of remedial works: (i) Gardesana tunnel exit; (ii) earth embankment with height of 4.5 m; (iii) deformable rockfall net; (iv) earth embankment with height of 6.0 m; (v) Gardesana tunnel entrance.

Table

Discontinuity Sets		Average orientation		Variability	
		Dip [°]	Dip direction [°]	Dip [°]	Dip direction [°]
South slope	K1	27	308	10–47	244–017
	K2	73	221	58–88	200–240
				85–88	026–059
	K3	78	153	61–88	142–166
				83–88	321–341
	K4	89	295	72–88	272–318
				72–88	090–135
North slope	K1	13	360	0–35	015–270
	K2	89	243	74–86	238–250
				79–82	051–067
	K3	84	143	75–87	141–150
				83–85	315–320
	K4	88	276	75–84	273–281
				85–87	098–105

Table 1: Joint sets identified on South and North slopes, respectively.

Zone	Sliding	Falling
1	100	000
2	-	001
3	101	001
4	100	000
5	-	001
6	110	010

Table 2. Key blocks computed for the six areas.